A comprehensively validated compact mechanism for dimethyl ether oxidation: an experimental and computational study

Rohit Sanjay Khare[a], P. Senthil Kumar[a], V. Raghavan[a], Krithika Narayanaswamy[a,*]

[a] *Thermodynamics and Combustion Engineering Laboratory, Department of Mechanical Engineering, Indian Institute of Technology Madras, Chennai – 600036, India*

Abstract

Dimethyl ether (DME) is regarded as one of the most promising alternatives to fossil fuels used in compression ignition engines. In order to critically evaluate its overall combustion behaviour via numerical simulations, an accurate as well as compact kinetic mechanism to describe its oxidation is most essential. In the present study, a short kinetic mechanism consisting of 23 species and 89 reactions is proposed to describe the oxidation of DME. This is based on the detailed San Diego mechanism. The short mechanism accurately reproduces the available experimental data for ignition delays, laminar flame speeds, and species profiles in flow reactors as well as jet-stirred reactors. To assess the validity of this reaction mechanism in non-premixed systems, extinction strain rates of DME-air mixtures, which are not available in the literature, are measured in a counter-flow diffusion flame burner as a part of the present work. The 23-species reaction mechanism is also able to predict the experimental data for extinction within the uncertainty limits. This mechanism is further reduced by introducing quasi-steady state assumptions for six intermediate species to finally obtain a 14-step global kinetic scheme. A code is developed in MATLAB to obtain these 14 global steps and their corresponding rate expressions in terms of the individual reaction rates. The 14-step mechanism performs as good as

*Corresponding Author
Email: krithika@iitm.ac.in

the 23-species mechanism for all the experimental data sets tested for.

Keywords: Dimethyl ether kinetics, Bottom-up approach, 23 species mechanism, Extinction, Quasi-steady state assumption, Reduced model

---

1. Introduction

Emissions from automobiles, especially that from compression ignition engines, significantly contribute to environmental pollution. An attractive way to tackle this problem is to use alternative fuels. Dimethyl ether (DME) is one such fuel, which can replace fossil diesel for use in compression ignition engines [1]. The high cetane number (55–60) [2] of DME and ease of its handling (remains a liquid when pressurized above 0.5 MPa) makes it particularly attractive for use in such applications [3]. The fast evaporation rate of DME leads to better mixing with air within the engine and its inherent oxygen content helps achieve smokeless combustion through reduced formation and high oxidation rates of particulates. In fact, diesel/DME blends have been shown to result in reduced soot precursors than neat diesel [2, 4–6].

Significant amount of research, both based on experiments and modeling, has been undertaken on DME kinetics [7–12]. Several detailed mechanisms have been proposed for DME oxidation. Dagaut *et al.* [7, 8] proposed a detailed reaction mechanism with 331 reactions involving 55 species to describe the low and high temperature oxidation of DME in a jet-stirred reactor (JSR) (550–1275 K, 1–10 atm) as well as the ignition of DME in shock tubes (650–1600 K, 3.5–40 bar). Curran *et al.* [9] developed a detailed kinetic model for DME oxidation and demonstrated its validity in JSR and shock tube configurations over a wide range of conditions (650–1300 K, 0.2–2.5, 1–40 atm). This model incorporated 336 reactions among 78 species. Some modifications were introduced to this kinetic scheme by Curran *et al.* [10] to additionally describe the oxidation of DME in a variable pressure flow reactor. Fischer *et al.* [11] further modified the mechanism proposed by Curran *et al.* [10] to extend its validity to include the pyrolysis of DME at high temperatures. Zhao *et al.* [12] developed a comprehensive model

for DME pyrolysis and oxidation in a hierarchial manner. This model, consisting of 290 reactions among 55 species, showed a good agreement against flow reactor, JSR data, shock tube ignition delays, and laminar flame speed measurements.

In a recent study, Burke *et al.* [13] proposed a detailed kinetic mechanism for DME oxidation by incorporating accurate rate constant measurements and calculations for the reactions of DME. The mechanism was also the first to employ a pressure-dependent treatment to the low temperature reactions of DME. It was validated using data available in the literature including, species profiles in flow reactor and JSR, shock tube ignition delay times, and flame speeds. Prince and Williams [14] came up with a 14-step DME sub-mechanism, to be combined with the San Diego mechanism [15], which was successfully tested against the aforementioned data sets as well. Dames *et al.* [16] developed a binary fuel kinetic model for DME and propane with focus on engine-relevant conditions (10–50 atm and 550–2000 K). The model (120 species and 711 reactions) was further validated against rapid compression machine (RCM) data for DME-propane mixtures.

Although detailed mechanisms provide accurate predictive capabilities, the computational time and complexities involved are large, which essentially constrains their use in multi-dimensional computations. This has propelled the development of compact reaction mechanisms for DME oxidation [17–22]. Cai *et al.* [17] proposed a reduced reaction mechanism, specifically to capture the autoignition of DME. Pan *et al.* [18] (29 species and 66 reactions), Yamada *et al.* [19] (23 species and 23 reactions), Kim *et al.* [20] (28 species and 45 reactions), and Chin *et al.* [21] (28 species) came up with skeletal/reduced models particularly applicable to engine combustion. Chang *et al.* [22] developed a reduced chemical mechanism for DME using a decoupling methodology, wherein the rate parameters in the DME sub-mechanism were optimized to match the experimental data (shock tubes, flow reactors, JSR data, and flame speeds). Nonetheless, the size of this mechanism (42 species and 171 reactions) remains comparable to some of the detailed mechanisms discussed above.

As discussed above, despite the availability of several short reaction mechanisms for DME oxidation, their range of validity is limited to specific configurations. However, in many combustion systems, the precise manner in which the combustion process advances is not known apriori. For instance, there may exist regions within a system where ignition and premixed flame propagation are dominant, while in others, diffusion governs the combustion process. Therefore, in order to be integrated with simulations of combustion systems in general, the short mechanism for DME oxidation should be applicable to a wide range of combustion configurations.

Thus, the objectives of this work are two-fold: (i) develop a short mechanism for DME oxidation that is as compact as possible, still containing the essential kinetics and (ii) ensure that the proposed mechanism is validated comprehensively to establish its ability to accurately predict a wide range of configurations of practical relevance to combustion. In view of the second objective, while significant data is available in literature for validation of DME kinetics in premixed environment, for instance, Refs. [7, 8, 10, 11, 13], there is a lack of experimental data in non-premixed systems. Thus, as a part of this work, extinction strain rates of DME-air mixtures have been obtained in a counter-flow non-premixed flame, thus expanding on the available database for kinetic model validation.

This work is organized as follows. First, the experimental methodology to measure extinction strain rates in a 1D laminar non-premixed counter-flow burner is presented (Section 2). Thereafter, following a similar approach to the development of a short kinetic model for methanol oxidation by Tarrazo *et al.* [23], a compact mechanism is developed for DME oxidation (discussed in Section 3). An extensive validation of the compact reaction scheme against available experimental data for constant volume and constant pressure homogeneous reactors, unstretched laminar premixed flames, and well-stirred reactor as well as the measured extinction strain rates is presented in Section 4. To further simplify this mechanism and subsequently reduce the computational cost when using in combustion simulations, quasi-steady state assumption has been

invoked for a few intermediate species. A reduced mechanism is thus arrived at for DME oxidation. Computations are performed to validate the results from this reduced mechanism against all experimental data sets (discussed in Section 5). Following this, the article is concluded by summarizing the contributions and highlighting the principal findings.

2. Counterflow Diffusion Flame Extinction Experiments

Significant data is available in literature for validating the DME kinetic model in a premixed environment, for instance, Refs. [7, 8, 10, 11, 13]. Along with configurations in a premixed system (such as shock tubes, flow reactors, and flame speeds), extinction strain rates in non-premixed flames are particularly important for validating a reaction scheme because it verifies the interplay between the time scales of kinetics and diffusion processes, which compete with each other during extinction. Wang *et al.* [24] obtained extinction strain rates of DME-oxygen mixtures at atmospheric pressure and elevated unburned mixture temperature in a counter-flow diffusion flame. Since most of the practical combustion systems use air as the oxidizer, as a part of the present work, experiments have been performed in a canonical 1D counter-flow configuration to obtain the extinction strain rates of DME-air mixtures in non-premixed flames. In the present work, strain rates at extinction are experimentally measured as a function of the mass fraction of fuel in the fuel stream ($Y_{F,1}$). This experimental data set acts as a validation target for the proposed short mechanism.

2.1. Experimental Apparatus

The counter-flow burner setup used in the present work is manufactured at UCSD and an exactly similar setup has been previously used by the UCSD group to measure the extinction and auto-ignition characteristics of several fuels [25, 26].

A schematic of the counter-flow burner setup used in the present study is shown in Fig. 1. It consists of fuel (bottom) and oxidizer (top) ducts, kept

co-axially opposing each other. The fuel duct ($d_f = 25.4$ mm) is surrounded by two concentric annular ducts. Nitrogen is supplied through the inner annular gap in order to minimize the effect of ambient interference. The outermost annular duct is connected to an exhaust system, which facilitates the suction of the hot product gases. The outer walls of this duct are provided with water spray nozzles (type BETE PJ15) to cool the hot product gases and thereby prevent their autoignition in the exhaust duct. Water is supplied to the spray nozzles through a mini centrifugal pump (TULLU AC-30). The oxidizer duct ($d_{ox} = 25.4$ mm) is surrounded by a concentric duct through which nitrogen is supplied, similar to that used in the fuel duct.

Plug-flow boundary condition is ensured by placing multiple stainless steel wire screens (200 meshes/inch) near the exits of both fuel and oxidizer ducts. The flow rates of DME, air and nitrogen are controlled using rotameters (with an uncertainty 2% of full scale reading). The fuel and nitrogen are mixed in a cylindrical mixing chamber of diameter 50 mm and length 200 mm. A series of fine stainless steel meshes are arranged inside the mixing chamber in order to ensure a homogeneous mixture.

2.2. Experimental Procedure

Before starting the experiment, the water cooling system is turned on. First, a stable flame is established by controlling the flow rate of DME through the fuel duct and by introducing a small pilot flame for ignition. The exhaust system is switched on immediately after the ignition to vent out hot products gases. Once the flame is stabilized, air is allowed to enter through the oxidizer duct to establish a flat flame as shown in Fig. 2(a). The curtain flow of nitrogen in both the ducts is adjusted using separate rotameters. The fuel is gradually diluted with nitrogen in the mixing chamber until the flame extinguishes, which is visually observed through several trials. The corresponding flowrates of DME, nitrogen, and air at extinction are recorded. The setup is then allowed to cool for sufficient amount of time before starting the next experimental trial. The

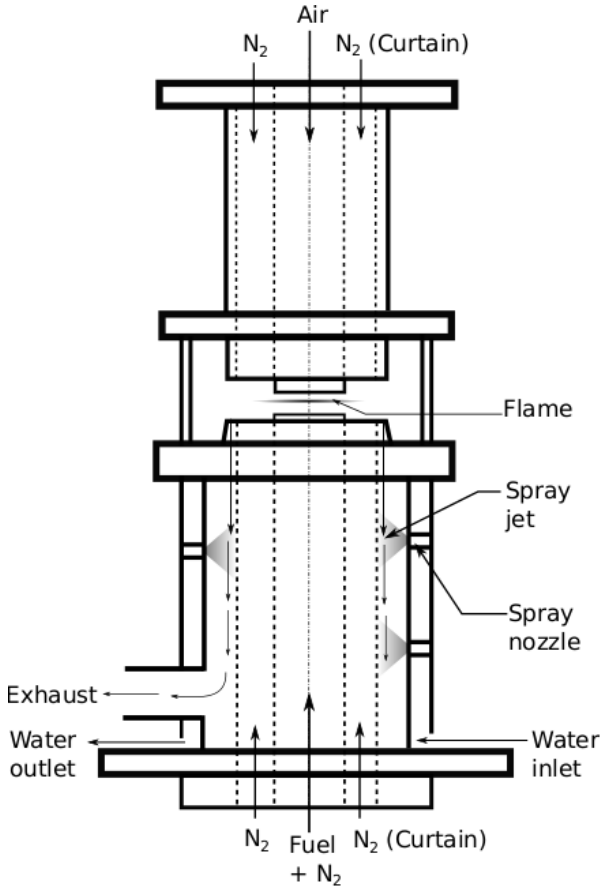

Figure 1: A schematic of the counter-flow diffusion flame burner.

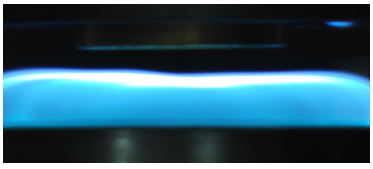

(a) 1D laminar DME-air counter-flow diffusion flame

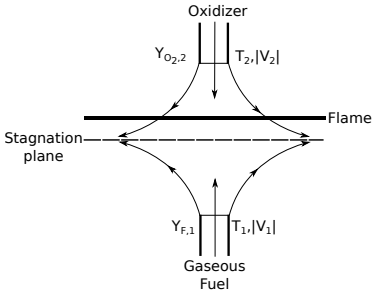

(b) Streamlines and flame location in a typical counter-flow burner

Figure 2: Details on counter-flow diffusion flame burner.

same procedure, is repeated to obtain the strain rates at extinction for different values of the fuel mass fraction in the fuel stream.

Keeping in mind the highly flammable and diffusive characteristics of DME when compared to other fuels, proper precautions have been taken while doing the experiments. Especially, the DME jet is ignited as quickly as possible and the exhaust system is switched on immediately after ignition.

Further, the momenta of the counterflowing reactant streams at the boundaries are kept almost equal to each other. This condition ensures that the stagnation plane formed by the two streams is approximately at the middle of the region between the two ducts. In the region between the stagnation plane and the oxidizer duct, the characteristic strain rate, a_2, defined as the normal gradient of the normal component of the flow velocity, evaluated at the stagnation plane, is given by [27],

$$a_2 = \frac{2|V_2|}{L}\left(1 + \frac{|V_1|\sqrt{\rho_1}}{|V_2|\sqrt{\rho_2}}\right).$$

Here, subscripts 1 and 2 denote the fuel and oxidizer side respectively (Fig. 2(b)), L denotes the distance between the two ducts, V the flow velocity normal to the stagnation plane and ρ represents the density. The average velocities of the reactants are estimated as the ratio of corresponding volumetric flow rates to the cross-section area of corresponding ducts.

All the experiments are carried out at atmospheric conditions. The separation distance between the fuel and oxidizer duct is maintained at 10 mm. The value of a_2 at extinction is denoted by $a_{2,E}$. The extinction strain rates have been obtained for different values of $\mathrm{Y_{F,1}}$ (fuel mass fraction on the fuel side), falling within 0.3–0.4, which is the range of values feasible using the present experimental setup. Throughout the experiments, $\mathrm{Y_{O_2,2}}$ (the mass fraction of oxygen on the oxidizer side) has a fixed value of 0.233. All the experiments have been repeated at least five times. The estimated uncertainty in $a_{2,E}$ is $\pm 12\%$ of the measured value. The experimental data is presented along with the results in Section 4.4.

As mentioned earlier, although a similar setup has been used previously by the UCSD group for measuring the critical conditions of extinction and auto-ignition, it is important to validate the present setup to account for the variability in the laboratory conditions. Thus, to examine the correctness of the experimental setup, the extinction data obtained in the present setup are compared against those obtained in the UCSD setup, and summarized in Table 1. The agreement between these data sets (within the estimated ±12% uncertainty) assures that the present setup is indeed suited and validated to measure extinction strain rates.

Table 1: Comparison between extinction strain rates obtained using the present counter-flow burner setup with those of the UCSD setup.

	Fuel and $Y_{F,1}$	UCSD Setup	Present Setup
Strain Rate at	(a) Methane, 0.18	200±20 [28]	205±25
Extinction (1/s)	(b) DME, 0.33	500±20 [29]	508±60

3. Mechanism Development

There are a number of techniques available for deriving a short mechanism from a detailed mechanism. Generally, a large detailed mechanism is reduced in stages by removing species and reactions that are insignificant to targets of interest until a smaller skeletal mechanism with the desired accuracy is obtained [30–35]. A different approach is adopted here to arrive at a short reaction model for DME oxidation following the lines of Tarrazo *et al.* [23]. This is essentially a "bottom-up approach" to incorporate just the necessary kinetics to describe the combustion characteristics with good fidelity. In the following discussion, the essential methodology behind the mechanism development is described specific to DME oxidation, nonetheless in a manner that is intuitive and suggestive to be adopted to any other fuel as well.

It is well known that the high temperature oxidation of DME (CH_3OCH_3) proceeds via:

$$CH_3OCH_3 \longrightarrow CH_3OCH_2 \longrightarrow \mathbf{CH_2O\ (+\ CH_3)} \longrightarrow \mathbf{HCO} \longrightarrow \mathbf{CO} \longrightarrow \mathbf{CO_2} \quad (1)$$

$$CH_3OCH_3 \longrightarrow CH_3O\ (+\ CH_3) \longrightarrow \mathbf{CH_2O} \longrightarrow \mathbf{HCO} \longrightarrow \mathbf{CO} \longrightarrow \mathbf{CO_2}, \quad (2)$$

in a similar manner to that of methanol (CH_3OH) [36];

$$CH_3OH \longrightarrow CH_2OH \longrightarrow \mathbf{CH_2O} \longrightarrow \mathbf{HCO} \longrightarrow \mathbf{CO} \longrightarrow \mathbf{CO_2}. \quad (3)$$

Therefore, a short mechanism for methanol proposed by Seiser *et al.* [37] is chosen as the starting point for the development of the DME mechanism in the present work. This 27-step mechanism by Seiser *et al.* [37] satisfactorily predicts the ignition times of methanol.

To obtain a base mechanism for DME oxidation, the reactions involving methanol and its immediate derivatives (methanol sub-mechanism) in the 27-step mechanism of Seiser *et al.* [37] are replaced by the 14-step DME sub-mechanism proposed by Prince and Williams [14]. Thus, in the resulting mechanism, the pathways for formaldehyde and its subsequent derivatives come from the 27-step Seiser model [37], while those for DME oxidation come from Prince and Willliams [14]. In addition to this, key reactions involving methyl (CH_3) radicals also need to be included, since these are particularly important for DME oxidation. This can be noted from pathways (1–3), where every DME molecule gives rise to a methyl radical (pathways (1) and (2)) as against none in methanol oxidation (pathway (3)).

In order to identify these reactions, firstly, the DME sub-mechanism by Prince and Williams [14] appended to the San Diego mechanism [15], is chosen as the *reference mechanism*. This choice is motivated by the relatively small size of the San Diego mechanism [14, 15] compared to other detailed models for DME oxidation ([12, 13]), which facilitates the kinetic analysis that is undertaken for the development of the present compact model. Further, the use of recent rate parameters in this model [14, 15] and its comprehensive validation

also makes it an appropriate choice as a reference mechanism for our study. Thereafter, a sensitivity analysis is performed at a wide range of operating conditions (ϕ: 0.5–2.5, T: 600–1300 K, P: 12–40 bar) with this reference mechanism and reactions R18, R20, R21, and R27 involving methyl radicals are thus identified as important for predicting ignition delays of DME-air mixtures. With the addition of these reactions to the base mechanism, the resulting kinetic scheme (*Mech_A*) consisting of 21 species and 51 reactions (counting forward and backward separately), is found to predict the ignition delays of DME-air mixtures accurately.

A series of simulations are carried out to assess the capability of this short mechanism to predict several combustion characteristics. In each of these, based on the predicted results, important reaction pathways have been identified and the short mechanism has been augmented with additional reactions. Such reactions are added to *Mech_A* from the well validated reference mechanism [14, 15] to extend its validity to premixed flame propagation, counter-flow non-premixed extinction, and homogeneous reactors. The reactions important for each configuration are identified based on the corresponding results of sensitivity and flux analysis performed using the reference mechanism. This approach results in a smaller mechanism as compared to the conventional approach, still ensuring accuracy, as will be demonstrated subsequently. The final short mechanism is listed in Table 2. The reactions from base mechanism and those added to extend the capability of the mechanism to predict different combustion configurations are shown in Table 2 clearly.

1D Laminar Premixed Flame. Laminar burning velocity is an important validation target for reaction mechanisms, which has been experimentally measured for DME-air mixtures at different equivalence ratios [38–41]. Results from brute force sensitivity analysis [38, 40] show that reactions involving CH_3 and HCO radicals are important to predict flame speeds accurately. Based on a sensitivity analysis conducted for lean, stoichiometric, and rich premixed flames at low and high pressures, the reactions R2, R3, R19, R22, R24, R33, R34, and

Table 2: Rate parameters in the Arrhenius form $k = AT^n \exp(-E_a/R_uT)$ for the 23 species mechanism. Units are mol, s, cm^3, kJ, and K.

No.	Reaction		A	n	E_a	Ref.
1	$H_2 + O \rightleftharpoons OH + H$		5.06×10^4	2.67	26.32	[42]
2	$H_2 + OH \rightleftharpoons H_2O + H$		1.17×10^9	1.30	15.21	[42]
3	$H + OH + M2 \rightleftharpoons H_2O + M2$		4.00×10^{22}	-2.00	0.00	[43]
4	$H_2O + O \rightleftharpoons 2\ OH$		7.00×10^5	2.33	60.87	[44]
5	$H + O_2 \rightleftharpoons OH + O$		3.52 x 10^{16}	-0.70	71.42	[45]
6	$H + O_2 + M1 \rightleftharpoons HO_2 + M1$	k_0	5.75×10^{19}	-1.40	0 .00	[43]
		k_∞	4.65×10^{12}	0.44	0.00	
7	$2\ HO_2 \rightarrow H_2O_2 + O_2$		1.03×10^{14}	0.00	46.20	[44]
			1.94×10^{11}	0.00	-5.895	
8	$HO_2 + OH \rightleftharpoons H_2O + O_2$		4.50×10^{14}	0.00	45.73	[46]
			7.00×10^{12}	0.00	-4.58	
9	$HO_2 + H \rightleftharpoons 2\ OH$		7.08×10^{13}	0.00	1.234	[47]
10	$HO_2 + O \rightarrow OH + O_2$		2.00×10^{13}	0.00	0.00	[48]
11	$HO_2 + H \rightleftharpoons H_2O + O$		3.10×10^{13}	0.00	7.20	[42]
12	$HO_2 + H \rightarrow H_2 + O_2$		1.66×10^{13}	0.00	3.443	[47]
13	$H_2O_2 + M3 \rightarrow 2\ OH + M3$	k_0	7.60×10^{30}	-4.20	213.68	[44]
		k_∞	2.63×10^{19}	-1.27	213.68	
14	$H_2O_2 + H \rightarrow HO_2 + H_2$		2.30×10^{13}	0.00	33.263	[49]
15	$H_2O_2 + OH \rightarrow H_2O + HO_2$		1.74×10^{12}	0.00	1.33	[44]
			7.59×10^{13}	0.00	30.43	
16	$H_2O_2 + H \rightarrow H_2O + OH$		1.00×10^{13}	0.00	15.00	[50]
17	$H_2O_2 + O \rightleftharpoons HO_2 + OH$		9.63×10^6	2.00	16.70	[50]
18	$CH_3 + O_2 \rightarrow CH_2O + OH$		3.30×10^{11}	0.00	37.41	[51]
19	$H + CH_3 + M9 \rightarrow CH_4 + M9$	k_0	2.47×10^{33}	-4.76	10.209	[52]
		k_∞	1.27×10^{16}	-0.63	1.602	
20	$CH_3 + HO_2 \rightarrow CH_3O + OH$		5.00×10^{12}	0.00	0.00	[53]
21	$2\ CH_3 + M8 \rightarrow C_2H_6 + M8$	k_0	1.27×10^{41}	-7.00	11.56	[54]
		k_∞	1.81×10^{13}	0.00	0.00	
22	$CH_3 + O \rightarrow CH_2O + H$		8.43×10^{13}	0.00	0.00	[53]
23	$2\ CH_3 \rightarrow C_2H_5 + H$		3.16×10^{13}	0.00	61.50	[55]
24	$CH_3 + OH \rightarrow CH_2O + H_2$		1.65×10^7	0.973	-8.41	[56]
25	$2\ CH_3 \rightarrow C_2H_4 + H_2$		1.00×10^{14}	0.00	133.90	[57]
26	$CH_4 + H \rightarrow CH_3 + H_2$		1.30×10^4	3.00	33.63	[54]
27	$CH_4 + O_2 \rightleftharpoons CH_3 + HO_2$		3.98×10^{13}	0.00	238.03	[58]
28	$CH_4 + OH \rightarrow CH_3 + H_2O$		1.60×10^7	1.83	11.64	[54]
29	$CO + OH \rightleftharpoons CO_2 + H$		4.40×10^6	1.50	-3.10	[48]
30	$CO + HO_2 \rightleftharpoons CO_2 + OH$		2.00×10^{13}	0.00	96.00	[49]
31	$CO + O + M14 \rightleftharpoons CO_2 + M14$	k_0	1.55×10^{24}	-2.79	17.535	[49]
		k_∞	1.80×10^{11}	0.00	9.975	

No.	Reaction		A	n	E_a	Ref.
32	$HCO + O_2 \rightarrow CO + HO_2$		7.58×10^{12}	0.00	1.715	[52]
33	$HCO + OH \rightarrow CO + H_2O$		3.00×10^{13}	0.00	0.00	[59]
34	$HCO + H \rightarrow CO + H_2$		5.00×10^{13}	0.00	0.00	[52]
35	$HCO + M4 \rightarrow CO + H + M4$		1.86×10^{17}	-1.00	71.13	[58]
36	$HCO + CH_3 \rightarrow CO + CH_4$		5.00×10^{13}	0.00	0.00	[52]
37	$CH_2O + OH \rightarrow HCO + H_2O$		3.90×10^{10}	0.89	1.70	[49]
38	$CH_2O + O \rightarrow HCO + OH$		3.50×10^{13}	0.00	14.70	[49]
39	$CH_2O + H \rightarrow HCO + H_2$		5.74×10^{7}	1.90	11.50	[60]
40	$CH_2O + HO_2 \rightarrow HCO + H_2O_2$		4.11×10^{4}	2.50	42.72	[61]
41	$CH_3O + O_2 \rightarrow CH_2O + HO_2$		4.28×10^{-13}	7.60	-14.80	[62]
42	$CH_3O + M5 \rightarrow CH_2O + H + M5$		7.78×10^{13}	0.00	56.54	[52]
43	$C_2H_4 + O \rightleftharpoons CH_3 + HCO$		2.25×10^{6}	2.08	0.00	[42]
44	$C_2H_5 + M11 \rightleftharpoons C_2H_4 + H + M11$	k_0	3.99×10^{33}	-4.99	167.36	[63]
		k_∞	1.11×10^{10}	1.037	153.84	
45	$C_2H_5 + O \rightarrow CH_3 + CH_2O$		4.24×10^{13}	0.00	0.00	[53]
46	$C_2H_5 + O_2 \rightarrow C_2H_4 + HO_2$		7.50×10^{14}	-1.00	20.083	[64]
47	$C_2H_5 + H \rightarrow C_2H_4 + H_2$		3.00×10^{13}	0.00	0.00	[53]
48	$C_2H_5 + O \rightleftharpoons C_2H_4 + OH$		3.06×10^{13}	0.00	0.00	[53]
49	$C_2H_6 + OH \rightarrow C_2H_5 + H_2O$		2.20×10^{7}	1.90	4.70	[53]
50	$C_2H_6 + O \rightarrow C_2H_5 + OH$		1.40	4.30	11.60	[53]
51	$C_2H_6 + M12 \rightarrow C_2H_5 + H + M12$	k_0	4.90×10^{42}	-6.43	448.339	[54]
		k_∞	8.85×10^{20}	-1.23	427.70	
52	$C_2H_6 + H \rightarrow C_2H_5 + H_2$		5.40×10^{2}	3.50	21.80	[53]
53	$C_2H_6 + CH_3 \rightarrow C_2H_5 + CH_4$		5.50×10^{-1}	4.00	34.70	[53]
54	$CH_3OCH_2 + O_2 \rightleftharpoons CH_3OCH_2O_2$		2.00×10^{12}	0.00	0.00	[12]
55	$CH_3OCH_2 + O_2 \rightarrow 2\ CH_2O + OH$		9.53×10^{10}	0.42	14.293	[65]
56	$CH_3OCH_2 \rightarrow CH_2O + CH_3$		1.20×10^{13}	0.00	107.738	[12]
57	$CH_3OCH_3 + OH \rightarrow CH_3OCH_2 + H_2O$		1.95×10^{7}	1.89	-1.531	[66]
58	$CH_3OCH_3 + HO_2 \rightarrow CH_3OCH_2 + H_2O_2$		2.68×10^{1}	0.00	69.036	[12]
59	$CH_3OCH_3 + CH_3 \rightarrow CH_3OCH_2 + CH_4$		2.68×10^{1}	3.778	40.297	[12]
60	$CH_3OCH_3 + M6 \rightleftharpoons CH_3O + CH_3 + M6$	k_0	1.72×10^{59}	-11.40	390.367	[66]
		k_∞	2.33×10^{19}	-0.66	352.038	
61	$CH_3OCH_3 + O_2 \rightleftharpoons CH_3OCH_2 + HO_2$		4.10×10^{13}	0.00	187.903	[12]
62	$CH_3OCH_3 + H \rightarrow CH_3OCH_2 + H_2$		3.94	4.13	7.448	[66]
63	$2\ CH_3OCH_2O_2 \rightarrow 2\ CH_3O + 2\ CH_2O + O_2$		1.307×10^{14}	-1.067	-1.533	[13]
64	$CH_3OCH_2O_2 \rightleftharpoons CH_2OCH_2O_2H$		2.20×10^{9}	0.00	66.30	[67]
65	$CH_2OCH_2O_2H \rightarrow 2\ CH_2O + OH$		1.50×10^{13}	0.00	85.772	[12]
66	$CH_2OCH_2O_2H + O_2 \rightarrow HO_2CH_2OCHO + OH$		2.86×10^{16}	-1.48	7.837	[13]
67	$HO_2CH_2OCHO \rightarrow CH_2O + CO_2 + OH + H$		2.50×10^{16}	0.00	179.912	[13]
68	$HO_2CH_2OCHO \rightarrow CH_2O + CO + 2\ OH$		2.50×10^{16}	0.00	179.912	[13]

The Chaperon efficiencies are provided in the mechanism file with the supplementary material.

R36 involving these species have been added to *Mech_A* above. It is important to note that the ignition delay predictions are not affected by the addition of these reactions, since ignition times are not largely sensitive to these pathways. Few other reactions that flame speeds are sensitive to, are already included in *Mech_A* since they are a part of the Seiser *et al.* [37] model, or the set of important reactions among methyl radicals identified earlier. Thus, this mechanism consisting of 21 species and 61 reactions (*Mech_B*) is found to accurately predict flame speeds and ignition delays.

Constant Pressure Homogeneous Reactor. When comparing against flow reactor data [10], it was found that the reference mechanism and *Mech_B* are unable to match the concentration profiles for the major species, particularly CO and H_2O, in the low temperature range of 550–600 K. Nonetheless, some of the existing detailed models, such as those proposed by Zhao *et al.* [12] and Burke *et al.* [13], are found to predict these results better (see Fig. S11 in supplementary material). Upon performing a reaction-flux analysis with these models [12, 13] at low temperatures, a pathway producing CO from the keto-hydroperoxide species (HO_2CH_2OCHO), given in a lumped form by,

$$HO_2CH_2OCHO \rightarrow CH_2O + CO + 2\ OH \text{ (R68 in Table 2)},$$

has been identified to be important for predicting the amounts of CO at these conditions. While the low temperature kinetics of DME in the reference mechanism [14] contains a parallel channel to produce CO_2 from HO_2CH_2OCHO (R67), the above route to form CO has been left out, and this is therefore absent in *Mech_B* as well.

In order to represent the amount of CO with better fidelity at low temperatures, the above reaction (R68) is now included in *Mech_B*. The rate parameters for the two parallel pathways forming CO (R68) and CO_2 (R67) are taken to be those of the entrance channel, keto-hydroperoxide $\longrightarrow$ OH + products [13], following the approach of Prince and Williams [14], nonetheless with the pre-exponential factor halved, thereby assigning equal importance to the two parallel

routes. In addition to the improvement in the amounts of CO at low temperatures, including R68 in *Mech_B* also results in a better agreement in the amounts of fuel, oxidizer, H_2O, and CO_2 at these temperatures, as will be demonstrated in Section 4. This lends confidence to the rate constants assigned to pathways R67 and R68.

Mech_B also fails to predict the amounts of CO at high temperatures. This disagreement has been traced to the incomplete description of consumption pathways for the intermediate species, H_2O_2 and CH_4. Based on results from reaction-flux analysis obtained using the reference mechanism, reactions R14–R17 for H_2O_2 and reactions R26 and R28 for CH_4, are added to *Mech_B* above. Further, reactions R30 and R31 have been added to achieve better accuracy on the computed amounts of carbon monoxide. It is found that the changes incorporated for the constant pressure homogeneous reactor do not affect the previously obtained flame speed results although, it slightly improves the low temperature ignition delays. This mechanism (*Mech_C*, consisting of 21 species and 73 reactions) accurately predicts all the data available in literature for DME oxidation in premixed combustion scenarios.

1D Laminar Counter-flow Diffusion Flame. An important component of the present work is to examine the extinction characteristics of DME fuelled non-premixed flames, where kinetics is strongly coupled with heat and mass transfer, and extend the validity of the short mechanism to this configuration as well. This is of practical relevance in systems where different modes of combustion could be manifest during the evolution of the combustion process. In the absence of fundamental extinction strain rate data, these have been obtained in this study in a counter-flow diffusion flame burner (discussed in Section 2). The reference mechanism predicts these experimental data within the uncertainty limits. However, *Mech_C* is found to underpredict the data over the entire experimental range. Sensitivity analysis towards peak temperatures using the reference mechanism reveal the importance of C_2H_4, C_2H_5, and C_2H_6 species. Out of these, C_2H_4 and C_2H_5 do not feature in *Mech_C*, while pathways for the

consumption of C_2H_6 are absent. Taking into account all of this, reactions R23, R25, and R43–R53 are added to *Mech_C*, which subsequently results in improved predictions for extinction strain rates when compared against the experimental data.

Thus, a short mechanism for DME oxidation, which consists of 89 reactions (counting forward and backward separately) among 23 chemical species (listed in Table 2) is obtained. The rate expressions for all the reactions are based on the San Diego mechanism [15] and the DME sub-mechanism from Prince and Williams [14]. These sources are indicated in Table 2. The thermochemical and transport data are also taken from these works [14, 15] as appropriate.

It should be noted that the short 14 step DME sub-mechanism by Prince and Williams [14] contains lumped reactions for the low temperature chemistry (reactions R61–R67). Apart from these, the rest are all elementary reactions. Further, it should be noted that few of the rate parameters related to the base chemistry in the San Diego mechanism [15] have been altered in their model to obtain better predictions against experimental data for smaller hydrocarbons. None of the rate parameters in the DME sub-mechanism by Prince and Williams [14] have been tuned to match any experimental data as explained in their original article. Thus, the proposed short model predominantly consists of elementary reactions, with rate parameters as reported by existing models in literature. Note that a chemical mechanism consisting primarily of elementary reactions offers two main advantages: (i) pressure and temperature dependence of elementary reactions are already captured in their rate expressions, and therefore, the model can be extended to conditions outside of the presented validation regime with relative ease, and (ii) model can be improved in a straightforward manner, by performing highly accurate calculations for the rate constants of the most sensitive reactions for a new configuration of interest.

Furthermore, this short mechanism, consisting of 23 species among 89 reactions, is found to be the smallest among the skeletal mechanisms proposed for DME oxidation. It is particularly interesting to also emphasize that further re-

moval of any species or reaction will not provide satisfactory results for at least one of the fundamental configurations discussed above. Thus, to summarize, this mechanism can be considered as the shortest and minimal possible model comprising predominantly of elementary reactions, with the rate parameters as reported by existing models in literature. This mechanism is referred to as the *23 species mechanism* in the rest of this article.

4. Results and Discussion

In this section, the simulations performed using the 23 species mechanism are compared against the experimental results for all the above mentioned configurations. The results obtained using the reference mechanism are also plotted along side to serve as a benchmark and thereby comment on the accuracy of the proposed short mechanism. Computations are performed using FlameMaster code, version 3.3.10 [68]. The boundary conditions specified in the computations are in accordance with those employed in the experiments.

4.1. Ignition Delay Times

Shock tubes are modeled as homogeneous, constant volume adiabatic reactors. The 23 species mechanism predicts the ignition delay times as good as the reference mechanism (Fig. 3) for all the ranges of equivalence ratios and pressures considered. Notably, it predicts ignition delays at low through high temperatures including the negative temperature coefficient behaviour, which is to be highlighted, given the compact size of the reaction scheme.

4.2. Laminar Flame Speeds

Laminar burning velocity is an important fundamental characteristic of a premixed fuel-air mixture within flammability limits. On a practical level, it affects the burning rate in internal combustion engines and therefore the engine's efficiency [69, 70] and emissions. It is therefore a useful target for kinetic mechanism validation in premixed scenario.

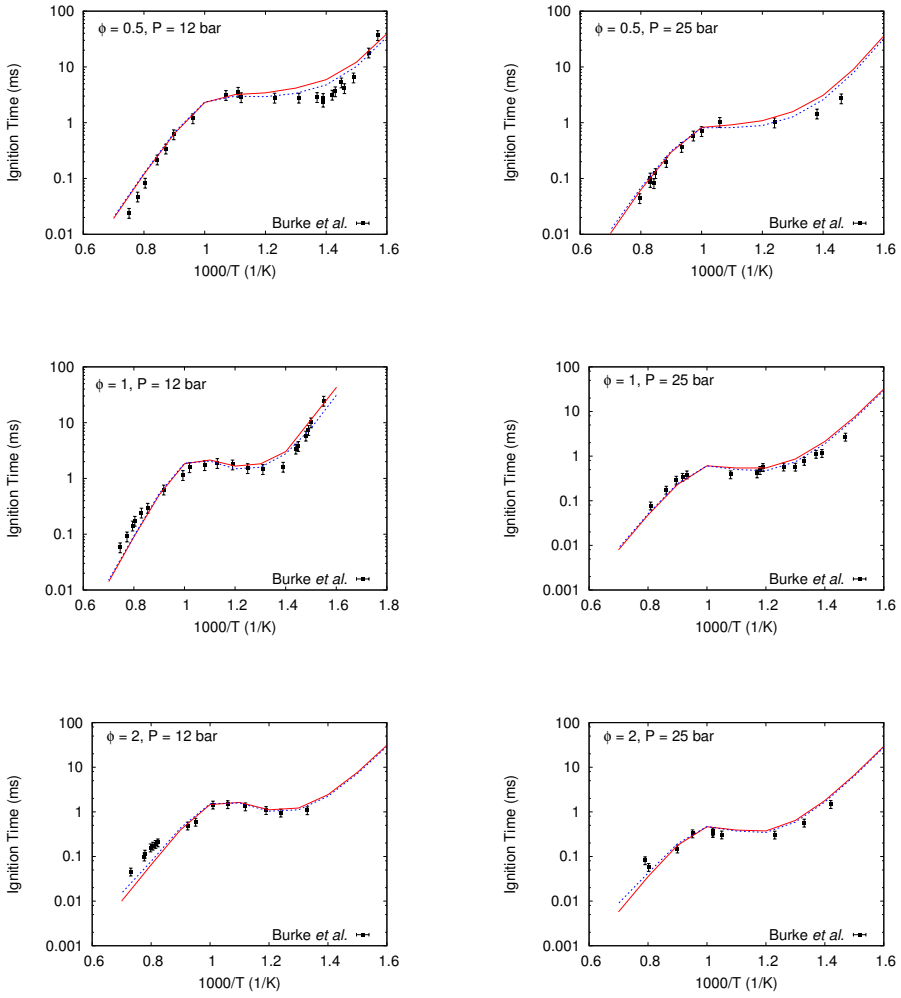

Figure 3: Ignition delay times of DME-air mixtures for a range of equivalence ratios (ϕ) and pressures. Symbols–experimental data from Burke *et al.* [13], lines –simulations: reference mechanism (solid lines), 23-species mechanism (dashed lines).

The laminar burning velocities have been evaluated as the eigenvalue of a system of 1D ordinary differential equations describing an adiabatic unstretched premixed flat flame [68]. Soret and Dufour effects are included in the calculations. The numerical results are ensured to be independent of the grid resolution, and the simulations are performed using second order central differencing for both convective and diffusion terms.

Zhao *et al.* [39] and Qin and Ju [40] have measured laminar flame speeds of DME-air mixtures using particle image velocimetry (stagnation flame burner configuration) and pressure-release type spherical bomb techniques, respectively. As shown in Fig. 4, the predictions using the 23 species model are in good agreement with the predictions of the reference model and lie within experimental uncertainties at atmospheric conditions. The 23 species as well as the reference model, under-predict the flame speeds of rich mixtures slightly at a higher pressure of 2 atm. Overall, the 23 species mechanism satisfactorily predicts the laminar burning velocities of DME-air mixtures.

Additionally, the results from the 23 species model are also compared against flame speciation data obtained in a burner-stabilized premixed flame [71]. These results which are shown in Fig. S8, demonstrate a good agreement between the predicted and experimental species profiles.

4.3. Species Concentration Profiles

Curran *et al.* [10] measured the major species observed in DME-air oxidation using a flow reactor. In the present work, these experiments have been modeled as a homogeneous and adiabatic constant pressure reactor and the results are shown in Fig. 5. It is clear that the 23 species mechanism reproduces the species profiles for the flow reactor configuration accurately.

The amounts of CO and H_2O, which are underpredicted by the reference mechanism, is well captured by the 23 species mechanism in the temperature range of 550–600 K (Figs. 5(c) and 5(d)). This improvement is attributed to the additional pathway R68 included in the 23 species mechanism. This is also

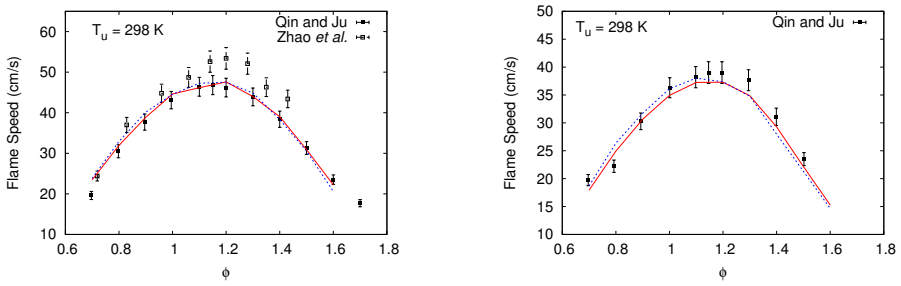

(a) P = 1 atm (b) P = 2 atm

Figure 4: Laminar burning velocities of DME-air mixtures at different equivalence ratios and pressures. Symbols – experiments: Qin and Ju [40] (filled symbols), Zhao *et al.* [39] (hollow symbols); lines – simulations: reference mechanism (solid lines), 23 species mechanism (dashed lines).

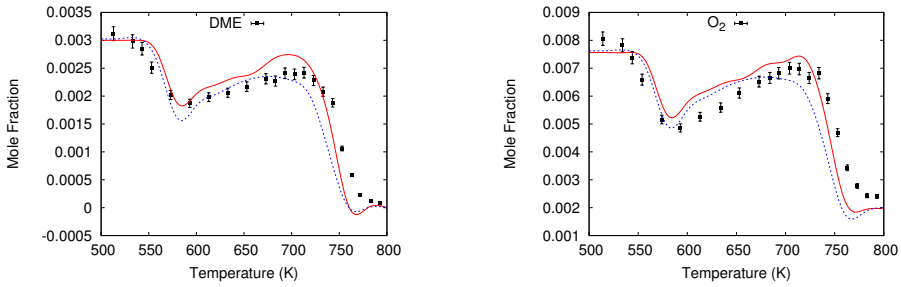

(a) Fuel (b) Oxidizer

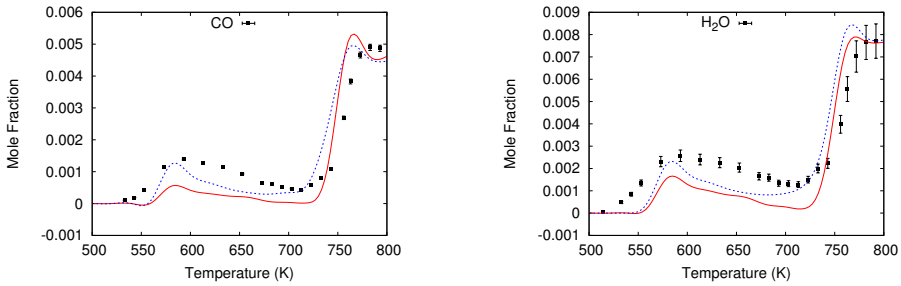

(c) Product: CO (d) Product: H_2O

Figure 5: Species profiles in a constant pressure flow reactor, $\phi = 1.19$, 0.3% DME in N_2 at 12.5 atm. Symbols – experimental data from Curran *et al.* [10]; lines – simulations: reference mechanism (solid lines), 23 species mechanism (dashed lines).

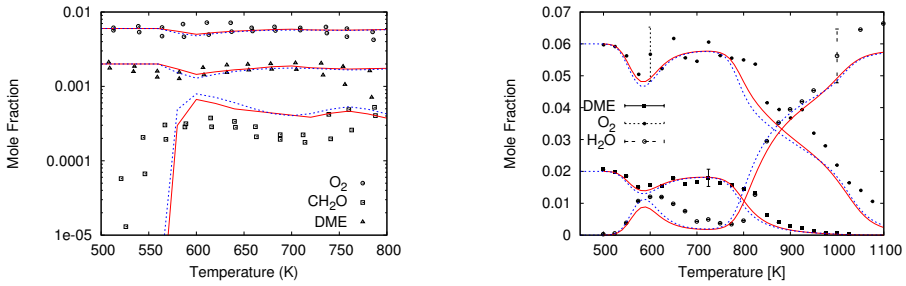

(a) 0.2% DME in N_2 at 10 atm, $\tau = 1$ s.

(b) 0.2% DME in He at 1 atm, $\tau = 2$ s.

Figure 6: Species profiles in a jet-stirred reactor at stoichiometric conditions. Symbols – experimental data from (a) Dagaut *et al.* [8], (b) Rodriguez *et al.* [72] with representative error bars; lines – simulations: reference mechanism (solid lines), 23-species mechanism (dashed lines).

supported by the simulated species–time histories of DME, O_2, CO, CO_2, and H_2O, at an initial temperature of 593 K (see Fig. S1).

The deviations between simulations and experimental data in CO and H_2O profiles, in the temperature range of 600–700 K shown in Fig. 5 are also observed with other detailed models for DME, such as the Zhao *et al.* [12] model and the recent Burke *et al.* [13] model (see Fig. S11), and warrants further investigation. The shift seen at ∼750 K in Fig. 5 should be taken with caution, since the temperature at which the rise/decay of species occurs, is found to depend on the residence time in the flow reactor, which is subject to uncertainties [10, 12] (see Fig. S2).

Dagaut *et al.* [8] and Rodriguez *et al.* [72] obtained species profiles in a jet-stirred reactor at stoichiometric conditions. Predictions from the 23 species model shows good agreement with these data sets as shown in Fig. 6. The 23 species mechanism is also validated against the recent atmospheric pressure jet-stirred reactor data by Moshammer *et al.* [73] and additional data by Rodriguez *et al.* [72], which span $\phi = 0.25$–2, $T = 500$–1100 K, and the data from Dagaut *et al.* [7] at $\phi = 1$ and $T = 900$–1200 K (see Figs. S3–S7). The model shows satisfactory agreement against all of these data sets.

4.4. Counter-flow Diffusion Flame Extinction

Figure 7 shows the extinction strain rates of DME-air mixtures measured as a function of fuel mass fraction. Overall, the extinction strain rates show an increasing trend with $Y_{F,1}$, suggesting that increasing heat release rate due to increasing amounts of fuel will require larger strain rates to achieve extinction. The extinction data obtained from the experiments is used to validate the reference and the 23 species mechanisms.

A one-dimensional counter-flow diffusion flame with steady plug-flow boundary conditions is used to simulate these experiments. The boundary conditions have been specified in accordance with the values used in the experiments. Figure 7 shows the comparison between the experimental values and the predictions using the two mechanisms. The reference mechanism as well as the 23 species mechanism predict the measured extinction strain rates within their reported uncertainties. This agreement verifies the applicability of the proposed 23 species model in non-premixed configurations as well.

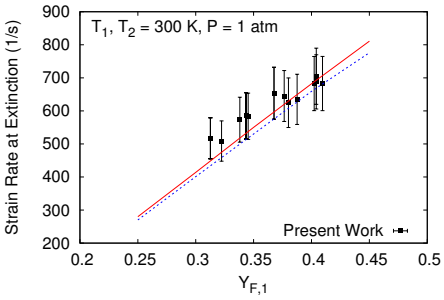

Figure 7: Extinction strain rate, $a_{2,E}$, as a function of fuel mass fraction, $Y_{F,1}$, of DME-air mixtures. Symbols – experiments: present work; lines – simulations: reference mechanism (solid lines), 23 species mechanism (dashed lines).

The results obtained using the 23 species model and the recent Burke *et al.* [13] model are shown in Figs. S9–S11, for representative cases, and are found to show a similar level of agreement. With the comprehensive assessment presented here, it can be concluded that the 23 species model (with 89 reactions)

developed and comprehensively assessed here can be employed to predict combustion parameters related to homogeneous (shock tubes, flow reactors, and JSRs) as well as heterogeneous (laminar flame speeds and non-premixed extinction) systems with confidence, yet retaining a compact size amenable to be integrated into realistic combustion simulations.

5. Reduced Reaction Mechanism

5.1. Introduction of Quasi-Steady State assumption

In order to reduce the short mechanism to a further reduced multi-step mechanism, quasi-steady state (QSS) assumption is invoked. Through this strategy, the differential equations for the evolution of certain species that can be assumed to exist in steady state (referred in short as *QSS species* in the following) are simplified into a set of algebraic equations, which are much faster to evaluate. A number of techniques are available in literature to systematically identify the suitable QSS species [74–76]. Lovas *et al.* [77, 78] proposed the Level of Importance (LOI) method, which is based on the instantaneous error in the concentration of a species set in steady state. In the present study, the QSS species are identified using the approach suggested by Pepiot [79], which is also based on the LOI method.

A code has been developed in MATLAB [80] to obtain a reduced mechanism upon introduction of quasi-steady state assumption, based on the work of Chen [81]. The 23 species mechanism, list of species to be set in steady state, and the set of reactions to eliminate (one for each QSS species) are provided as an input to the code. The reduced mechanism along with the rate expressions for each global reaction in terms of the individual reaction rates is returned as the output. The code is made available online at `https://bitbucket.org/ccube_iitm/qss_reduction`.

In the present 23 species mechanism for DME oxidation, the set of intermediate species, HO_2, CH_3, HCO, CH_3O, CH_3OCH_2, and $CH_2OCH_2O_2H$ are

identified as suitable QSS species. The fast reactions, R9, R19, R36, R41, R54, and R66, are chosen to be eliminated corresponding to these species, since the slow reactions are rate limiting. With these as input to the code discussed above, a 14-step reduced mechanism for DME is obtained, and this is listed in Table 3. The rates of the global reactions (W_i) in terms of the individual reaction rates (w_i) are given in Table 4.

Table 3: 14 step reduced mechanism obtained upon setting six intermediate species (HO_2, CH_3, HCO, CH_3O, CH_3OCH_2, and $CH_2OCH_2O_2H$) in steady state within the 23 species mechanism proposed in the present work.

No.	Global Reaction
I	$2\ OH \rightleftharpoons H_2 + O_2$
II	$2\ H + H_2O_2 \rightleftharpoons H_2 + 2\ OH$
III	$OH + CH_4 \rightleftharpoons H_2 + H + CH_2O$
IV	$2\ CH_4 \rightleftharpoons H_2 + 2\ H + C_2H_4$
V	$H + H + M \rightleftharpoons H_2 + M$
VI	$CH_2O \rightleftharpoons H_2 + CO$
VII	$H + C_2H_5 \rightleftharpoons H_2 + C_2H_4$
VIII	$H + C_2H_6 \rightleftharpoons H_2 + C_2H_5$
IX	$H + O_2 + CH_3OCH_3 \rightleftharpoons H_2 + CH_3OCH_2O_2$
X	$OH + H + M \rightleftharpoons H_2O + M$
XI	$O + H_2O \rightleftharpoons 2\ OH$
XII	$OH + CO \rightleftharpoons H + CO_2$
XIII	$CH_3OCH_2O_2 \rightleftharpoons OH + 2\ CH_2O$
XIV	$O_2 + CH_3OCH_2O_2 \rightleftharpoons OH + HO_2CH_2OCHO$

The concentrations of the steady state species are obtained in terms of the remaining species by equating their rates of production and consumption. For our specific case, explicit expressions cannot be obtained for the concentrations of the QSS species, since some of them are coupled (participate in the same reac-

Table 4: Rate expressions (W_i) for the 14 global steps in terms of w_i. Here, w_i refers to the net reaction rate of the i^{th} reaction in the 23 species mechanism (listed in Table 2).

No.	Rate Expression
W_I	$-w_5 - w_6 - w_{18} - w_{20} - w_{27} - w_{32} - w_{46} - w_{61} - w_{63} - w_{68} + w_7 + w_8 + w_{10} + w_{12} + w_{42} + w_{56}$
W_{II}	$-w_7 - w_{40} - w_{58} + w_{13} + w_{14} + w_{15} + w_{16} + w_{17}$
W_{III}	$-w_{56} - w_{60} + w_{18} + w_{20} + w_{22} + w_{24} + w_{43} + w_{45}$
W_{IV}	$-w_{43} - w_{45} + w_{21} + w_{23} + w_{25}$
W_V	$-w_1 - w_2 - w_8 - w_{10} - w_{13} - w_{15} - w_{16} - w_{17} - w_{22} - w_{37} - w_{38} - w_{42} - w_{43} - w_{44} - w_{45} - w_{48} - w_{49} - w_{50} - w_{51} - w_{53} - w_{57} - w_{59} + w_5 + w_6 + w_{21} + w_{26} + w_{27} + w_{32} + w_{34} + w_{63}$
W_{VI}	$w_{37} + w_{38} + w_{39} + w_{40} + w_{43} + w_{67} + w_{68}$
W_{VII}	$-w_{21} - w_{23} + w_{44} + w_{45} + w_{46} + w_{47} + w_{48}$
W_{VIII}	$-w_{21} + w_{49} + w_{50} + w_{51} + w_{52} + w_{53}$
W_{IX}	$w_{57} + w_{58} + w_{59} + w_{60} + w_{61} + w_{62}$
W_X	$-w_5 + w_1 + w_2 + w_3 + w_8 + w_{10} + w_{15} + w_{16} + w_{17} + w_{22} + w_{28} + w_{31} + w_{33} + w_{37} + w_{38} + w_{43} + w_{45} + w_{48} + w_{49} + w_{50} + w_{57}$
W_{XI}	$-w_5 - w_{11} + w_1 + w_4 + w_{10} + w_{17} + w_{22} + w_{31} + w_{38} + w_{43} + w_{45} + w_{48} + w_{50}$
W_{XII}	$w_{29} + w_{30} + w_{31} + w_{67}$
W_{XIII}	$w_{55} + w_{56} + w_{60} + w_{63} + w_{65} + w_{67} + w_{68}$
W_{XIV}	$-w_{65} - w_{67} - w_{68} + w_{64}$

tion as reactants and/or products). This results in a set of non-linear algebraic equations to be solved to obtain the amounts of QSS species.

5.2. Results

The 14 step reduced mechanism has been evaluated against all the data sets, which the 23 species model has been validated for. The computations are performed in FlameMaster [68] by setting the QSS species identified above in

steady state. Figure 8 shows representative results for ignition delays, species profiles in flow reactor, premixed and non-premixed flames.

A careful examination of these results show that the reduced mechanism agrees very well with all the experimental data with similar accuracy as that of the 23 species mechanism. This also verifies the suitability of species chosen above to prevail in steady state. Thus, with the proposed 14 step reduced mechanism, reduction in computational cost can be achieved, while retaining the same accuracy as that of the 23 species mechanism.

6. Conclusion

In this work, as a first major contribution, to expand on the database for kinetic validation of DME oxidation in a non-premixed environment, extinction strain rates of DME-air mixtures have been measured in counter-flow diffusion flames. Further, a short mechanism has been developed for DME oxidation using a "bottom-up approach". Starting with a 27 step mechanism developed for methanol ignition by Seiser *et al.* [37], reaction steps are added from the reference San Diego mechanism [14, 15] (chosen as a reference model for analysis) with the help of sensitivity and reaction-flux analysis in order to improve upon results for ignition delays, flame speeds, species profiles, and extinction strain rates.

The essential methodology behind the mechanism development is described specific to DME oxidation, nonetheless in a manner that is intuitive and suggestive to be adopted to any other fuel molecule as well. This mechanism consisting of 23 species and 89 reactions (counting forward and reverse separately) has been comprehensively validated against the available experimental data in premixed configurations and the predictions are in good agreement with these data sets. This short model is also found to predict the extinction strain rates within the experimental uncertainties, thereby, providing evidence of its applicability in a transport dominated system, in addition to kinetically dominated systems.

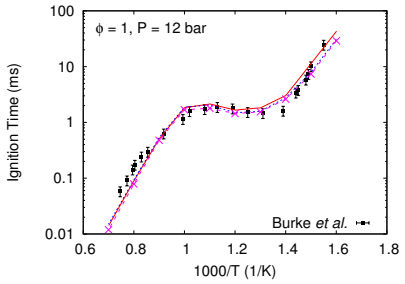

(a) Shock tube ignition delay predictions. Symbols – experimental data from Burke *et al.* [13], lines – simulations.

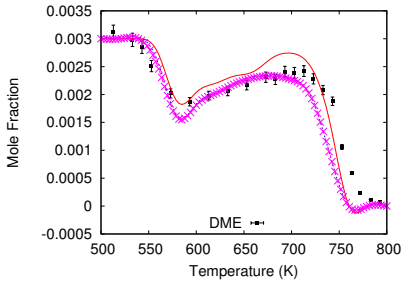

(b) Computed fuel concentration profile in a flow reactor, $\phi = 1.19$, 0.3% DME in N_2 at 12.5 atm. Symbols – experimental data from Curran *et al.* [10]; lines – simulations.

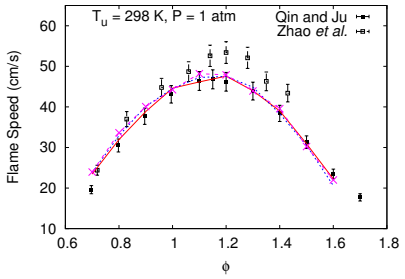

(c) Laminar burning velocities for DME-air mixtures at atmospheric pressure. Symbols – Experiments: Qin *et al.* [40] (filled symbols), Zhao *et al.* [39] (hollow symbols); lines – simulations.

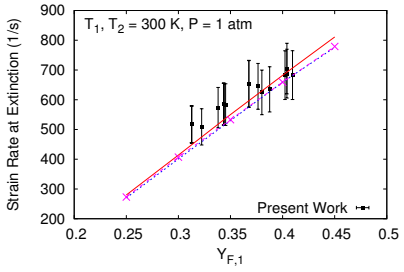

(d) Extinction strain rate, $a_{2,E}$, as a function of fuel mass fraction, $Y_{F,1}$, for DME-air mixtures. Symbols – experiments: present work; lines – simulations.

Figure 8: Predictions with the 14 step mechanism for shock tubes, flow reactors, premixed and non-premixed flames. In all the figures: reference mechanism (solid lines), 23 species mechanism (dashed lines), 14 step mechanism (dashed-crossed lines).

To summarize, a comprehensively validated 23 species model has been arrived at for DME oxidation, which is the smallest such kinetic model in the literature consisting predominantly of elementary steps with the rate parameters based on existing models in literature.

Furthermore, a reduction code has been developed to reduce any given skeletal mechanism by introducing QSS assumption for few of the intermediate species. The source code is made available online at `https://bitbucket.org/ccube_iitm/qss_reduction`. A 14-step reduced mechanism has been obtained by setting suitable intermediate species in steady state. This kinetic scheme is also found to be in good agreement with the experimental results. Both the 23 species and 14 step mechanisms reproduce the available experimental data with good accuracy in all the configurations considered. Thus, the compact kinetic schemes for the oxidation of DME developed here can be applied to a wide range of experimental conditions and configurations with acceptable accuracy and reduced computational cost. The 23 species mechanism as well as the associated thermodynamic and transport properties are provided with the supplementary material.

Acknowledgements

The authors would like to thank the National Center for Combustion Research and Development (NCCRD) for procurement of the counter-flow burner setup. The last author gratefully acknowledges support from the New Faculty Initiation Grant, Project No. MEE/15-16/845/NFIG offered by the Indian Institute of Technology Madras. The first and the last author would also like to thank Dr. Perrine Pepiot at Cornell University for sharing the source code for identifying quasi-steady state species. The authors also gratefully acknowledge Prof. Kalyanasundaram Seshadri from the University of California San Diego for helping us to manufacture the opposed flow burner at UCSD and for insightful discussions on the experiments conducted in the counter-flow burner.

References

[1] S.C. Sorenson, Dimethyl ether in diesel engines: progress and perspectives, ASME J. Eng. Gas Turb. Power 123 (2001) 652–658.

[2] T. Fleisch, C. McCarthy, A. Basu, C. Udovich, P. Charbonneau, W. Slodowske, S.E. Mikkelsen, J. McCandless, A new clean diesel technology: demonstration of ulev emissions on a navistar diesel engine fueled with dimethyl ether, SAE (1995), paper 950061.

[3] C. Arcoumanis, C. Bae, R. Crookes, E. Kinoshita, The potential of dimethyl ether (dme) as an alternative fuel for compression-ignition engines: A review, Fuel 87 (2008) 1014–1030.

[4] E.M. Chapman, A.L. Boehman, P. Tijm, F. Waller, Emission characteristics of a navistar 7.3 l turbodiesel fueled with blends of dimethyl ether and diesel fuel, SAE (2001), paper 2001-01-3226.

[5] R. Khare, V. Raghavan, K. Narayanaswamy, A chemical kinetic modeling study of the effects of oxygenated species on soot emissions from diesel engines, Proceedings of the International Conference on Sustainable Energy and Environmental Challenges (2017), paper 023.

[6] C.K. Westbrook, W.A. Pitz, H.J. Curran, Chemical kinetic modeling study of the effects of oxygenated hydrocarbons on soot emissions from diesel engines, J. Phys. Chem. 110 (2006) 6912–6922.

[7] P. Dagaut, J. Boettner, M. Cathonnet, Chemical kinetic study of dimethylether oxidation in a jet stirred reactor from 1 to 10 atm: Experiments and kinetic modeling, Symp. (Int.) Combust. 26 (1996) 627–632.

[8] P. Dagaut, C. Daly, J.M. Simmie, M. Cathonnet, The oxidation and ignition of dimethylether from low to high temperature (500–1600 K): Experiments and kinetic modeling, Symp. (Int.) Combust. 27 (1998) 361–369.

[9] H.J. Curran, W.J. Pitz, C.K. Westbrook, P. Dagaut, J.C. Boettner, M. Cathonnet, A wide range modeling study of dimethyl ether oxidation, Int. J. Chem. Kinet. 30 (1998) 229–241.

[10] H.J. Curran, S.L. Fischer, F.L. Dryer, The reaction kinetics of dimethyl ether. ii: low-temperature oxidation in flow reactors, Int. J. Chem. Kinet. 32 (2000) 741–759.

[11] S.L. Fischer, F.L. Dryer, H.J. Curran, The reaction kinetics of dimethyl ether. i: high-temperature pyrolysis and oxidation in flow reactors, Int. J. Chem. Kinet. 32 (2000) 713–740.

[12] Z. Zhao, M. Chaos, A. Kazakov, F.L. Dryer, Thermal decomposition reaction and a comprehensive kinetic model of dimethyl ether, Int. J. Chem. Kinet. 40 (2008) 1–18.

[13] U. Burke, K.P. Somers, P. OToole, C.M. Zinner, N. Marquet, G. Bourque, E.L. Petersen, W.K. Metcalfe, Z. Serinyel, H.J. Curran, An ignition delay and kinetic modeling study of methane, dimethyl ether, and their mixtures at high pressures, Combust. Flame 162 (2015) 315–330.

[14] J.C. Prince, F.A. Williams, A short reaction mechanism for the combustion of dimethyl-ether, Combust. Flame 162 (2015) 3589–3595.

[15] The San Diego Mechanism, Version 2016-08-15, `http://web.eng.ucsd.edu/mae/groups/combustion/mechanism.html`.

[16] E.E. Dames, A.S. Rosen, B.W. Weber, C.W. Gao, C.J. Sung, W.H. Green, A detailed combined experimental and theoretical study on dimethyl ether/propane blended oxidation, Combust. Flame 168 (2016) 310–330.

[17] J. Beeckmann, L. Cai, O. Röhl, H. Pitsch, N. Peters, A reduced kinetic reaction mechanism for the autoignition of dimethyl ether, SAE (2010), paper 2010-01-2108.

[18] L. Pan, S. Kokjohn, Z. Huang, Development and validation of a reduced chemical kinetic model for dimethyl ether combustion, Fuel 160 (2015) 165–177.

[19] H. Yamada, H. Sakanashi, N. Choi, A. Tezaki, Simplified oxidation mechanism of DME applicable for compression ignition, SAE (2003), paper 2003-01-1819.

[20] H. Kim, S. Cho, K. Min, Reduced chemical kinetic model of DME for HCCI combustion, SAE (2003), paper 2003-01-1822.

[21] G.T. Chin, J.Y. Chen, V.H. Rapp, R.W. Dibble, Development and validation of a reduced DME mechanism applicable to various combustion modes in internal combustion engines, J. Combust. 2011 (2011).

[22] Y. Chang, M. Jia, Y. Zhang, Y. Li, W. Fan, M. Xie, Development of a reduced chemical mechanism for dimethyl ether (DME) using a decoupling methodology, SAE (2017), paper 2017-01-2191.

[23] E. Fernández-Tarrazo, M. Sánchez-Sanz, A.L. Sánchez, F.A. Williams, A multipurpose reduced chemical-kinetic mechanism for methanol combustion, Combust. Theor. Model. 20 (2016) 613–631.

[24] Y.L. Wang, P.S. Veloo, F.N. Egolfopoulos, T.T. Tsotsis, A comparative study on the extinction characteristics of non-premixed dimethyl ether and ethanol flames, Proc. Combust. Inst. 33 (2011) 1003–1010.

[25] R. Seiser, S. Humer, K. Seshadri, E. Pucher, Experimental investigation of methanol and ethanol flames in nonuniform flows, Proc. Combust. Inst. 31 (2007) 1173–1180.

[26] R. Seiser, L. Truett, D. Trees, K. Seshadri, Structure and extinction of non-premixed n-heptane flames, Symp. (Int.) Combust. 27 (1998) 649–657.

[27] K. Seshadri, F.A. Williams, Laminar flow between parallel plates with injection of a reactant at high Reynolds number, Int. J. Heat Mass Transfer 21 (1978) 251–253.

[28] P. Mairhofer, G. Mairinger, K. Seshadri, X.S. Bai, R. Seiser, E. Pucher, Rate-ratio asymptotic analysis of the influence of stoichiometric mixture fraction on structure and extinction of laminar, nonpremixed methane flames with comparison to experiments, Proc. Combust. Inst. 36 (2017) 1495–1503.

[29] M.H. Gall, G. Mairinger, R. Khare, K. Narayanaswamy, V. Raghavan, K. Seshadri, The Influence of Stoichiometric Mixture Fraction on Extinction of Laminar, Nonpremixed DME Flame, 10^{th} U.S. Combustion Meeting 2017.

[30] M. Frenklach, Reduction of chemical reaction models, Numer. Approaches Combust. Model. 135 (1991) 129–154.

[31] T. Lu, C.K. Law, A directed relation graph method for mechanism reduction, Proc. Combust. Inst. 30 (2005) 1333–1341.

[32] K.E. Niemeyer, C.J. Sung, M.P. Raju, Skeletal mechanism generation for surrogate fuels using directed relation graph with error propagation and sensitivity analysis, Combust. Flame 157 (2010) 1760–1770.

[33] P. Pepiot-Desjardins, H. Pitsch, An efficient error-propagation-based reduction method for large chemical kinetic mechanisms, Combust. Flame 154 (2008) 67–81.

[34] A.S. Tomlin, T. Turányi, M.J. Pilling, Mathematical tools for the construction, investigation and reduction of combustion mechanisms, Compr. Chem. Kinet. 35 (1997) 293–437.

[35] P. Pepiot-Desjardins, H. Pitsch, An automatic chemical lumping method for the reduction of large chemical kinetic mechanisms, Combust. Theor. Model. 12 (2008) 1089–1108.

[36] C.K. Westbrook, F.L. Dryer, Chemical kinetic modeling of hydrocarbon combustion, Prog. Energy Combust. Sci. 10 (1984) 1–57.

[37] R. Seiser, K. Seshadri, F.A. Williams, Detailed and reduced chemistry for methanol ignition, Combust. Flame 158 (2011) 1667–1672.

[38] C.A. Daly, J.M. Simmie, J. Würmel, N. DjebaÏli, C. Paillard, Burning velocities of dimethyl ether and air, Combust. Flame 125 (2001) 1329–1340.

[39] Z. Zhao, A. Kazakov, F.L. Dryer, Measurements of dimethyl ether/air mixture burning velocities by using particle image velocimetry, Combust. Flame 139 (2004) 52–60.

[40] X. Qin, Y. Ju, Measurements of burning velocities of dimethyl ether and air premixed flames at elevated pressures, Proc. Combust. Inst. 30 (2005) 233–240.

[41] Z. Huang, Q. Wang, J. Yu, Y. Zhang, K. Zeng, H. Miao, D. Jiang, Measurement of laminar burning velocity of dimethyl ether–air premixed mixtures, Fuel 86 (2007) 2360–2366.

[42] D.L. Baulch, C.J. Cobos, R.A. Cox, C. Esser, P. Frank, T. Just, J.A. Kerr, M.J. Pilling, J. Troe, R.W. Walker, Evaluated kinetic data for combustion modelling, J. Phys. Chem. Ref. Data 21 (1992) 411–734.

[43] P. Saxena, F.A. Williams, Testing a small detailed chemical-kinetic mechanism for the combustion of hydrogen and carbon monoxide, Combust. Flame 145 (2006) 316–323.

[44] E. Fernández-Tarrazo, A.L. Sánchez, F.A. Williams, Hydrogen-air mixing-layer ignition at temperatures below crossover, Combust. Flame 160 (2013) 1981–1989.

[45] D.A. Masten, R.K. Hanson, C.T. Bowman, Shock tube study of the reaction H2 + OH = OH + O using OH laser absorption, J. Phys. Chem. 94 (1990) 7119–7128.

[46] Z. Hong, K.Y. Lam, R. Sur, S. Wang, D.F. Davidson, R.K. Hanson, On the rate constants of OH + HO2 and HO2 + HO2: A comprehensive study of H2O2 thermal decomposition using multi-species laser absorption, Proc. Combust. Inst. 34 (2013) 565–571.

[47] M.A. Mueller, T.J. Kim, R.A. Yetter, F.L. Dryer, Flow reactor studies and kinetic modeling of the H2/O2 reaction, Int. J. Chem. Kinet. 31 (1999) 113–125.

[48] J. Warnatz, Rate coefficients in the C/H/O system, Combust. Chem. Springer (1984) 197–360.

[49] M.L. Rightley, F.A. Williams, Structures of CO diffusion flames near extinction, Combust. Sci. Technol. 125 (1997) 181–200.

[50] R.A. Yetter, F.L. Dryer, H. Rabitz, A comprehensive reaction mechanism for carbon monoxide/hydrogen/oxygen kinetics, Combust. Sci. Technol. 79 (1991) 97–128.

[51] R. Zellner, F. Ewig, Computational study of the methyl+ oxygen chain branching reaction, J. Phys. Chem. 92 (1988) 2971–2974.

[52] P. Saxena, Numerical and experimental studies of ethanol flames and autoignition theory for higher alkanes, PhD thesis, University of California, San Diego, 2007.

[53] M. Frenklach, H. Wang, M.J. Rabinowitz, Optimization and analysis of large chemical kinetic mechanisms using the solution mapping method-combustion of methane, Prog. Energy Combust. Sci. 18 (1992) 47–73.

[54] J.C. Hewson, F.A. Williams, Rate-ratio asymptotic analysis of methane–air diffusion-flame structure for predicting production of oxides of nitrogen, Combust. Flame 117 (1999) 441–476.

[55] K.P. Lim, J.V. Michael, The thermal reactions of CH3, Technical report, Argonne National Lab 1994.

[56] A.W. Jasper, S.J. Klippenstein, L.B. Harding, B. Ruscic, Kinetics of the reaction of methyl radical with hydroxyl radical and methanol decomposition, J. Phys. Chem. 111 (2007) 3932–3950.

[57] Y. Hidaka, T. Nakamura, H. Tanaka, K. Inami, H. Kawano, High temperature pyrolysis of methane in shock waves and rates for dissociative recombination reactions of methyl radicals and for propyne formation reaction, Int. J. Chem. Kinet. 22 (1990) 701–709.

[58] R.P. Lindstedt, G. Skevis, Chemistry of acetylene flames, Combust. Sci. Technol. 125 (1997) 73–137.

[59] W. Tsang, R.F. Hampson, Chemical kinetic data base for combustion chemistry. part i. methane and related compounds, J. Phys. Chem. Ref. Data 15 (1986) 1087–1279.

[60] E.A. Irdam, J.H. Kiefer, L.B. Harding, A.F. Wagner, The formaldehyde decomposition chain mechanism, Int. J. Chem. Kinet. 25 (1993) 285–303.

[61] B. Eiteneer, C.L. Yu, M. Goldenberg, M. Frenklach, Determination of rate coefficients for reactions of formaldehyde pyrolysis and oxidation in the gas phase, J. Phys. Chem. 102 (1998) 5196–5205.

[62] S.C. Li, F.A. Williams, Formation of nox, ch4, and c2 species in laminar methanol flames, Symp. (Int.) Combust. 27 (1998) 485–493.

[63] Y. Feng, J.T. Niiranen, A. Bencsura, V.D. Knyazev, D. Gutman, W. Tsang, Weak collision effects in the reaction C2H5 = C2H4 + H, J. Phys. Chem. 97 (1993) 871–880.

[64] J.C. Prince, F.A. Williams, Short chemical-kinetic mechanisms for low-temperature ignition of propane and ethane, Combust. Flame 159 (2012) 2336–2344.

[65] C.M. Rosado-Reyes, J.S. Francisco, J.J. Szente, M.M. Maricq, and L.F. Østergaard, Dimethyl ether oxidation at elevated temperatures (295-600 k), J. Phys. Chem. 109 (2005) 10940–10953.

[66] R. Sivaramakrishnan, J.V. Michael, A.F. Wagner, R. Dawes, A.W. Jasper, L.B. Harding, Y. Georgievskii, S.J. Klippenstein, Roaming radicals in the thermal decomposition of dimethyl ether: Experiment and theory, Combust. Flame 158 (2011) 618–632.

[67] K. Suzaki, N. Kanno, K. Tonokura, M. Koshi, K. Tsuchiya, A. Tezaki, Formation of ho2 and oh in photolytically initiated oxidation of dimethyl ether, Chem. Phys. Letters 425 (2006) 179–184.

[68] H. Pitsch, M. Bollig, FlameMaster v3.3.10: A computer code for homogeneous combustion and one-dimensional laminar flame calculations, 1998.

[69] J.T. Farrell, W. Weissman, R.J. Johnston, J. Nishimura, T. Ueda, Y. Iwashita, Fuel effects on SIDI efficiency and emissions, SAE (2003), 2003-01-3186.

[70] T.W. Klio, What causes slower flame propagation in the lean-combustion engine, J. Eng. Gas Turb. Power 112 (1990) 349.

[71] T.A. Cool, J. Wang, N. Hansen, P.R. Westmoreland, F.L. Dryer, Z. Zhao, A. Kazakov, T. Kasper, K. Kohse-Höinghaus, Photoionization mass spectrometry and modeling studies of the chemistry of fuel-rich dimethyl ether flames, Proc. Combust. Inst. 31 (2007) 285–293.

[72] A. Rodriguez, O. Frottier, O. Herbinet, R. Fournet, R. Bounaceur, C. Fittschen, F. Battin-Leclerc, Experimental and modeling investigation of the low-temperature oxidation of dimethyl ether, J. Phys. Chem. 119 (2015) 7905–7923.

[73] K. Moshammer, A.W. Jasper, V. Popolan, M. Denisia, Z. Wang, V.S. Shankar, L. Ruwe, C.A. Taatjes, P. Dagaut, N. Hansen, Quantification of the keto-hydroperoxide (HOOCH2OCHO) and other elusive intermediates during low-temperature oxidation of dimethyl ether, J. Phys. Chem. 140 (2016) 7890–7910.

[74] C.J. Montgomery, M.A. Cremer, J.Y. Chen, B. Berkeley, C.K. Westbrook, L.Q. Maurice, Reduced chemical kinetic mechanisms for hydrocarbon fuels, J. Propul. Power 18 (2002) 192–198.

[75] T. Turanyi, A.S. Tomlin, M.J. Pilling, On the error of the quasi-steady-state approximation, J. Phys. Chem. 97 (1993) 163–172.

[76] J.Y. Chen, Automatic generation of reduced mechanisms and their applications to combustion modeling, Trans. Aero. Astro. Soc. Rep. China 33 (2001) 59–67.

[77] T. Løvås, P. Amnéus, F. Mauss, E. Mastorakos, Comparison of automatic reduction procedures for ignition chemistry, Proc. Combust. Inst. 29 (2002) 1387–1393.

[78] T. Løvås, D. Nilsson, F. Mauss, Automatic reduction procedure for chemical mechanisms applied to premixed methane/air flames, Proc. Combust. Inst. 28 (2000) 1809–1815.

[79] P. Pepiot, Automatic strategies to model transportation fuel surrogates, PhD thesis, Stanford University, 2008.

[80] MATLAB 2016, The mathworks, Natick MA USA.

[81] J.Y. Chen, A general procedure for constructing reduced reaction mechanisms with given independent relations, Combust. Sci. Technol. 57 (1988) 89–94.